*LETTER* Communicated by Aaditya Rangan

# Continuation-Based Numerical Detection of After-Depolarization and Spike-Adding Thresholds

**Jakub Nowacki**
*jakub.nowacki@tessella.com*
*Tessella, Abingdon, OX14 3YS, U.K.*

**Hinke M. Osinga**
*h.m.osinga@auckland.ac.nz*
*Department of Mathematics, University of Auckland, Auckland 1142, New Zealand*

**Krasimira T. Tsaneva-Atanasova**
*k.tsaneva-atanasova@bristol.ac.uk*
*Bristol Centre for Applied Nonlinear Mathematics, Department of Engineering Mathematics, University of Bristol, Bristol BS8 1TR, U.K.*

**The changes in neuronal firing pattern are signatures of brain function, and it is of interest to understand how such changes evolve as a function of neuronal biophysical properties. We address this important problem by the analysis and numerical investigation of a class of mechanistic mathematical models. We focus on a hippocampal pyramidal neuron model and study the occurrence of bursting related to the after-depolarization (ADP) that follows a brief current injection. This type of burst is a transient phenomenon that is not amenable to the classical bifurcation analysis done, for example, for periodic bursting oscillators. In this letter, we show how to formulate such transient behavior as a two-point boundary value problem (2PBVP), which can be solved using well-known continuation methods. The 2PBVP is formulated such that the transient response is represented by a finite orbit segment for which onsets of ADP and additional spikes in a burst can be detected as bifurcations during a one-parameter continuation. This in turn provides us with a direct method to approximate the boundaries of regions in a two-parameter plane where certain model behavior of interest occurs. More precisely, we use two-parameter continuation of the detected onset points to identify the boundaries between regions with and without ADP and bursts with different numbers of spikes. Our 2PBVP formulation is a novel approach to parameter sensitivity analysis that can be applied to a wide range of problems.**

## 1 Introduction

The firing patterns in neurons are an important feature that is generally associated with specific brain functions (Llinás, 1988). Under various

 

conditions, many neurons tend to fire bursts, that is, clusters of high-frequency spikes (Krahe & Gabbiani, 2004). Bursts are generated in response to stimuli, which can be electrical (Yue & Yaari, 2004; Brown & Randall, 2009) or chemical (Rinzel, 1985; Tsaneva-Atanasova, Sherman, van Goor, & Stojilkovic, 2007) and occur periodically or as single events. The bursting activity is characterized by slow alterations between near-steady-state behavior, the so-called silent phase, and the active phase when clusters of spikes are fired (Rinzel, 1987). This bursting behavior plays an important role in many phenomena, namely, synaptic plasticity (Thomas, Watabe, Moody, Makhinson, & O'Dell, 1998), transmission of stimulus-related information (Krahe & Gabbiani, 2004), and sensory system function (Martinez-Conde, Macknik, & Hubel, 2002). It is not only limited to controlled in vitro experiments, but has also been reported to occur in-vivo. For instance, spiking and bursting behavior has been documented in in-vivo recordings from a single place cell (Lee, Manns, Sakmann, & Brecht, 2006; Harvey, Collman, Dombeck, & Tank, 2009; Epsztein, Brecht, & Lee, 2011). In addition, such firing patterns are reported to take place in pathological conditions such as epilepsy (McCormick & Contreras, 2001) and Alzheimer's disease (Brown, Chin, Leiser, Pangalos, & Randall, 2011). Even relatively small changes in biophysical properties of neurons (Brown & Randall, 2009; Nowacki, Osinga, Brown, Randall, & Tsaneva-Atanasova, 2011; Brown et al., 2011) or their morphology (van Elburg & van Ooyen, 2010) can have a large impact on the neuron's excitable behavior. Therefore, when using mathematical models for studying such firing patterns, it is essential to consider different sets of parameters because parameter uncertainty is common in these models.

We present a method that allows the analysis of transient processes. In contrast to periodic bursting, transients bursts are challenging to address with standard bifurcation methods, which are designed for long-term behavior. Periodic bursters, also called bursting oscillators, have been studied extensively (see Rinzel, 1987; Terman, 1991; Guckenheimer, Gueron, & Harris-Warrick, 1993; Izhikevich, 2000; Govaerts & Dhooge, 2002; Guckenheimer, Tien, & Willms, 2005; Tsaneva-Atanasova, Osinga, Riess, & Sherman, 2010; Ermentrout & Terman, 2010). Here, a parameter-driven modification of firing patterns, such as spike adding, is associated with so-called fold bifurcations of these periodic orbits (Terman, 1991; Osinga & Tsaneva-Atanasova, 2010; Tsaneva-Atanasova et al., 2010). In this letter, we are interested in spike adding and bursting as a transient behavior, which is known to occur, for example, in hippocampal pyramidal neurons (Andersen, Morris, Amaral, Bliss, & O'Keefe, 2007; Brown & Randall, 2009; Nowacki et al., 2011). In this case, a neuron is stimulated briefly, that is, perturbed away from its resting potential, and bursting takes place during the return to this equilibrium state. Due to the uniqueness of solutions in deterministic systems, the firing patterns that arise from prescribed

perturbations away from equilibrium cannot coexist. Hence, parameter-driven modifications such as spike adding cannot be associated with fold bifurcations of periodic orbits, and classical bifurcation methods used for identifying different bursting patterns in mathematical models cannot be applied in the context of transient behavior. Nevertheless, the underlying spike-adding mechanism via a canard-like phase is the same as for periodic orbits. Indeed, we have already presented a detailed slow-fast analysis of this behavior using elements of geometric singular perturbation theory (Nowacki, Osinga, & Tsaneva-Atanasova, 2012).

In this letter, we focus on the numerical detection of transient firing patterns in our system. We show how one can associate a type of bifurcation or sequence of bifurcations with the phenomenon of spike adding in a transient burst. As in Nowacki et al. (2012), we view the response of the system to a short current injection as a finite-time orbit segment that is the solution of a two-point boundary value problem (2PBVP). The parameter dependence of such solutions can then be studied using the numerical continuation of the solutions to this 2PBVP. The 2PBVP setup we use in our approach is quite general and can be applied to many transient bursting patterns. Our primary motivation for developing this method is to study transient bursting related to so-called after-depolarization (ADP) and how it depends on neuronal biophysical properties. The phenomenon of ADP is empirically defined as a positive deflection of the membrane potential after a spike, which creates a characteristic hump (Izhikevich, 2006). A series of additional spikes on top of ADP is generated if the membrane potential crosses a bursting threshold during the ADP (Brown & Randall, 2009; Nowacki et al., 2011). In this letter, we consider the ADP to be the positive deflection of the membrane potential after the last spike triggered by the short current injection. We use the 2PBVP formulation to define the onsets of ADP and a spike, such that these onsets can be detected as fold bifurcations in a one-parameter continuation of the 2PBVP. A subsequent two-parameter fold continuation establishes curves in a two-parameter plane that approximates the boundaries between regions of different bursting behaviors in the model and identifies the excitability threshold.

We consider a model of pyramidal neurons as a case study to illustrate the approximation of onsets of ADP and bursts with our numerical method. This case study is a bursting neuron model that uses four general classes of fast and slow, inward and outward currents in Hodgkin-Huxley formalism (Hodgkin & Huxley, 1952) and has been systematically derived through careful comparison to a detailed pyramidal cell model (Nowacki et al., 2011). The main feature that we exploit in our study is a natural timescale separation in the model. The majority of classical work on periodic spiking and bursting behavior (e.g., Rinzel, 1987; Terman, 1991; Guckenheimer et al., 1993; Izhikevich, 2000) emphasizes the pivotal role

of the slow variables for governing these behaviors. We find that we can also make use of this timescale separation when characterizing the onset of ADP or the threshold for a new spike. Indeed, both onsets of ADP and a spike can be approximated as extrema of a slow variable of the system. We explain in detail how to formulate the problem such that one can detect the extremum as a fold bifurcation with respect to a system variable, which is not achievable using the standard fold detection with respect to parameters. As a result, we are able to perform a one-parameter fold detection and two-parameter fold continuation of the 2PBVP over a large region of interest in the two-parameter plane. The advantage of our approach is that the numerical method automatically identifies a parameter-dependent and state-dependent excitability threshold as part of the computation.

Parameter continuations may be particularly important for model predictions that take into account the effects of parameters that currently cannot be controlled in an experimental environment. Our approach is very efficient, because we characterize the boundaries between regions of ADP and other excitable behavior in such a way that they can be detected directly and continued numerically in a two-parameter setting. This means that we compute the boundary explicitly as a one-dimensional curve rather than identifying it implicitly in a brute-force exploration of the entire two-parameter plane. Based on our analysis, we are able to describe the implications of changes to model parameters for excitability.

This letter is organized as follows. In the next section, we present our model of study. In section 3, we formulate the problem as a 2PBVP and show how to constrain the system such that the solutions correspond to those at a threshold. We discuss both the onsets of ADP and a spike in sections 3.1 and 3.2, respectively, and show how to detect these as folds in a one-parameter continuation. We continue these folds in two parameters in section 4 and obtain an overview of the regions of different model behaviors. We then provide a detailed investigation of the model behavior at and near the boundaries of these regions. We end with conclusions in section 5. The numerical computations are performed with the package Auto (Doedel, 1981; Doedel & Oldeman, 2009) and visualizations are done in Python (Oliphant, 2007) using Matplotlib (Hunter, 2007).

## 2 The Model

We use the model from Nowacki et al. (2012) as a case study to illustrate our new numerical method for detection and subsequent continuation of the onsets of ADP or a spike. This model is a simplified version of the physiological model of hippocampal pyramidal neurons presented in Nowacki et al. (2011) and considers general classes $I_{\mathrm{FI}}$, $I_{\mathrm{SI}}$, $I_{\mathrm{FO}}$, and $I_{\mathrm{SO}}$ of fast and slow, inward, and outward currents in Hodgkin-Huxley formalism (Hodgkin &

Table 1: Default Parameter Values for the Simplified Pyramidal Neuron Model Equation 2.1.

| | $C_m = 1.0\,\mu\text{F/cm}^2$ | |
|---|---|---|
| | Inward Currents | Outward Currents |
| | $E_I = 80.0$ mV | $E_0 = -80.0$ mV |
| Fast | $g_{FI} = 2.0$ mS/cm$^2$ | |
| | $V_{m_{FI}} = -25.0$ mV | |
| | $k_{m_{FI}} = 5.0$ mV | |
| | $g_{SI} = 0.5$ mS/cm$^2$ | $g_{FO} = 9.5$ mS/cm$^2$ |
| | $V_{m_{SI}} = -54.0$ mV | $V_{m_{FO}} = -6.0$ mV |
| | $k_{m_{SI}} = 5.0$ mV | $k_{m_{FO}} = 11.5$ mV |
| | $\tau_{m_{SI}} = 3.0$ ms | $\tau_{m_{FO}} = 1.0$ ms |
| Slow | | $g_{SO} = 1.2$ mS/cm$^2$ |
| | $V_{h_{SI}} = -56.0$ mV | $V_{m_{SO}} = -20.0$ mV |
| | $k_{h_{SI}} = 8.5$ mV | $k_{m_{SO}} = 10.0$ mV |
| | $\tau_{h_{SI}} = 20.0$ ms | $\tau_{m_{SO}} = 75.0$ ms |

Huxley, 1952). The model is five-dimensional and has the form

$$\begin{cases} \dfrac{dV}{dt} = \dfrac{1}{C_m}\Big[-g_{FI}\, m_{FI_\infty}(V)\,(V - E_I) - g_{SI}\, m_{SI}^2\, h_{SI}\,(V - E_I), \\ \qquad\qquad -g_{FO}\, m_{FO}\,(V - E_O) - g_{SO}\, m_{SO}\,(V - E_O) + I_{app}\Big], \\ \dfrac{dx}{dt} = \dfrac{x_\infty(v) - x}{\tau_x}, \end{cases} \tag{2.1}$$

where $x \in \{m_{SI}, m_{FO}, m_{SO}, h_{SI}\}$; here, we assume that the fast inward current is instantaneous. We use the Boltzmann form

$$x_\infty(v) = \frac{1}{1 + \exp\left(-\frac{V - V_x}{k_x}\right)}, \tag{2.2}$$

for the relevant activation and inactivation steady-state functions $m_{FI_\infty}(V)$, $m_{SI_\infty}(V)$, $m_{FO_\infty}(V)$, $m_{SO_\infty}(V)$, and $h_{SI_\infty}(V)$. The parameters used are the same as in Nowacki et al. (2012), unless specified otherwise; these default values are also given in Table 1 for convenience.

System 2.1 is capable of reproducing a broad range of cell responses typically observed in experiments (see Nowacki et al., 2011; Brown & Randall, 2009; Golomb, Yue, & Yaari, 2006; Yue, Remy, Su, Beck, & Yaari, 2005). Here, we mimic the experiment where a current is injected for only a short time. If

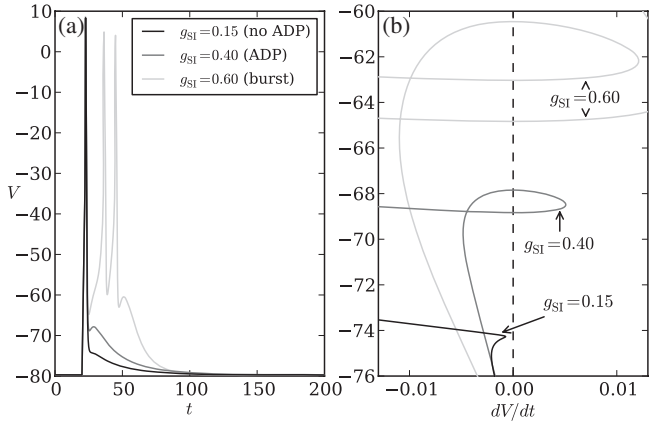


Figure 1: Three responses of system 2.1 to a current injection applied at $t =$ 20 ms of strength $I_{app} = 20\,\mu\text{A/cm}^2$ and duration 3 ms, where $g_{\text{SI}}$ (in $\text{mS/cm}^2$) takes the values $g_{\text{SI}} = 0.15$, $g_{\text{SI}} = 0.40$, and $g_{\text{SI}} = 0.60$. (a) The resulting time series of the membrane potential $V$. (b) An enlargement in the $(dV/dt,\ V)$-plane of the region of interest near the $V$-nullcline (vertical dashed line).

the injected current is strong enough, then one or more spikes are generated during the transient phase, where the system returns to its resting potential. For our numerical experiment, we set $I_{app} = 20\,\mu\text{A/cm}^2$ and apply it to system 2.1 over a time interval of 3 ms, which ensures that the membrane potential $V$ rises to a fully developed spike before the current is turned off.

Figure 1a depicts the time series of $V$ for three such experiments, where the conductance $g_{\text{SI}}$ of the slow inward current is set to the three successive values of 0.15, 0.40, and $0.60\,\text{mS/cm}^2$. The injected current is applied at $t =$ 20 ms, and the resulting first spike is almost the same for each of the three responses. However, the subsequent behavior, after the applied current has been turned off, clearly depends on the choice of $g_{\text{SI}}$. The responses for $g_{\text{SI}} = 0.40\ \text{mS/cm}^2$ (middle curve) and $g_{\text{SI}} = 0.60\,\text{mS/cm}^2$ (top curve) exhibit ADP, while the response for $g_{\text{SI}} = 0.15\,\text{mS/cm}^2$ (bottom curve) is a spike without ADP.

The occurrence of ADP can easily be defined as a crossing of the $V$-nullcline (Nowacki et al., 2011); we illustrate this in Figure 1b, where we plot the responses in the projection onto the $(dV/dt,\ V)$ plane and focus on the activity near the $V$-nullcline, that is, the vertical dashed line at $dV/dt = 0$. As explained previously (Nowacki et al., 2011), at the onset of ADP, the membrane potential has a cubic tangency, which means that the response, when projected onto the $(dV/dt, V)$-plane, makes a quadratic tangency with the $V$-nullcline. The response without ADP, for $g_{\text{SI}} = 0.15\,\text{mS/cm}^2$, lies entirely to the left of the $V$-nullcline in Figure 1b, while the (middle) response

for $g_{SI} = 0.40\,\mathrm{mS/cm^2}$ exhibits a nonmonotonic loop and $dV/dt > 0$ during the short rise time of ADP. A second cubic tangency develops as $g_{SI}$ increases from $0.40\,\mathrm{mS/cm^2}$ to $0.60\,\mathrm{mS/cm^2}$, so that the response for $g_{SI} = 0.60\,\mathrm{mS/cm^2}$ in Figure 1b crosses the $V$-nullcline multiple times. Note that the ADP after the last spike is qualitatively the same as that for $g_{SI} = 0.40\,\mathrm{mS/cm^2}$.

The presence of ADP is a precursor for generating a spike, and we expect that the respective onsets of ADP and a new spike occur close together in parameter space. In the next section, we explain how to detect both onsets numerically.

## 3 Excitability Thresholds as a Boundary Value Problem

We formulate the onset of ADP and the thresholds of each new spike in a burst as two-point boundary value problems (2PBVP) in such a way that a standard numerical continuation package can be used. We implemented our approach using Auto (Doedel, 1981; Doedel & Oldeman, 2009), but other continuation packages, such as the recently developed package CoCo (Dankowicz & Schilder, 2009, 2011), would be suitable as well.

The setup in Auto is rather similar to the computational approach taken in Nowacki et al. (2012), but there is an important difference in the definition of the boundary conditions. In Nowacki et al. (2012), we analyzed the geometrical mechanism of spike adding and investigated how the transient response of system 2.1 was tracing the slow manifolds of the underlying fast subsystem. Since the transitions between responses with a different number of spikes occur over exponentially small parameter intervals, we used 2PBVP continuation to capture the topological changes of the response, which would be virtually impossible to compute using initial-value integration. However, the 2PBVP setup in Nowacki et al. (2012) does not identify the moment of the spike-adding transitions; it only characterizes these transitions from a geometrical point of view. For completeness, we formulate the 2PBVP again here and point readers who are familiar with the setup in Nowacki et al. (2012) to the difference in formulating the boundary conditions 3.6 and 3.7 that determine the total integration time for the orbit segment, respectively.

As is standard in Auto, we consider an orbit segment $\mathbf{u} = \mathbf{u}(t)$ defined on the time interval $0 \le t \le 1$. For $t \in [0, 1]$, we define $\mathbf{u}(t) = [V(tT), m_{SI}(tT), m_{FO}(tT), m_{SO}(tT), h_{SI}(tT)]$ as the five-dimensional phase-space vector in system 2.1, which is a solution of

$$\mathbf{u}' = T\,\mathbf{f}(\mathbf{u}, \lambda, I_{app}). \tag{3.1}$$

Here, $\mathbf{f} : \mathbb{R}^5 \times \mathbb{R}^k \times \mathbb{R}$ is the continuously differentiable right-hand side of system 2.1. The time rescaling to the $[0, 1]$ interval has the effect that the total

required integration time $T$ appears as a parameter in equation 3.1 (see also Nowacki et al., 2012). The parameter vector $\lambda \in \mathbb{R}^k$ essentially represents the parameters of interest; we focus on the maximal conductances $g_{SI}$ and $g_{FO}$ of the slow inward and fast outward currents. However, additional parameters will be introduced to obtain a well-posed 2PBVP, so that $\lambda$ typically consists of more than two parameters. The applied current $I_{app}$ is specified separately in equation 3.1, and we consider two consecutive orbit segments, denoted $\mathbf{u}_{ON}$ and $\mathbf{u}_{OFF}$, such that $\mathbf{u}_{ON}$ satisfies equation 3.1 with $I_{app} = 20\,\mu\text{A/cm}^2$ and $\mathbf{u}_{OFF}$ satisfies equation 3.1 with $I_{app} = 0\,\mu\text{A/cm}^2$.

More precisely, we consider the system of equations

$$\mathbf{u}'_{ON}(t) = T_{ON}\ \mathbf{f}\big(\mathbf{u}_{ON}(t), \lambda, I_{app}\big), \tag{3.2}$$

$$\mathbf{u}'_{OFF}(t) = T_{OFF}\,\mathbf{f}(\mathbf{u}_{OFF}(t), \lambda, 0), \tag{3.3}$$

where the end point $\mathbf{u}_{ON}(1)$ of $\mathbf{u}_{ON}$ is the starting point $\mathbf{u}_{OFF}(0)$ of $\mathbf{u}_{OFF}$. That is, we require the boundary condition

$$\mathbf{u}_{ON}(1) - \mathbf{u}_{OFF}(0) = 0. \tag{3.4}$$

The short current injection is supposed to perturb system 3.1 from its resting potential. Hence, the begin point $\mathbf{u}_{ON}(0)$ of $\mathbf{u}_{ON}$ should be equal to the stable equilibrium of system 3.1 with $I_{app} = 0$, which we can solve for implicitly by imposing the boundary condition

$$\mathbf{f}(\mathbf{u}_{ON}(0), \lambda, 0) = 0. \tag{3.5}$$

Note that system 3.2 and 3.3 with boundary conditions 3.4 and 3.5 is effectively an initial value problem that has a well-defined unique solution as soon as the two integration times $T_{ON}$ and $T_{OFF}$ have been specified. The nature of the short current injection is such that $T_{ON}$ is fixed (we set $T_{ON} = 3\,\text{ms}$). The idea is to restrict $T_{OFF}$ in such a way that the solution to equations 3.2 to 3.5 is determined by the onset of ADP or the onset of a spike. Indeed, both ADP and additional bursting take place after the current has been switched off; hence, they are a characterization of the orbit segment $\mathbf{u}_{OFF}$. Figure 2 illustrates the setup with an example where we defined $\mathbf{u}_{OFF}$ with the additional constraint that $\mathbf{u}_{OFF}(1)$ lies at a local maximum, denoted $P$; this local maximum $P$ is preceded by a local minimum, denoted B, and indicates the presence of ADP. The concatenation of $\mathbf{u}_{ON}$ and $\mathbf{u}_{OFF}$ in original time coordinates is shown with the time series of $V$ in Figure 2a. This combined trajectory is a solution of system 2.1 with $I_{app}$ following the short-current-injection protocol. We consider the trajectory in Figure 2a only up to time $T_{ON} + T_{OFF}$; the gray line indicates the extended trajectory

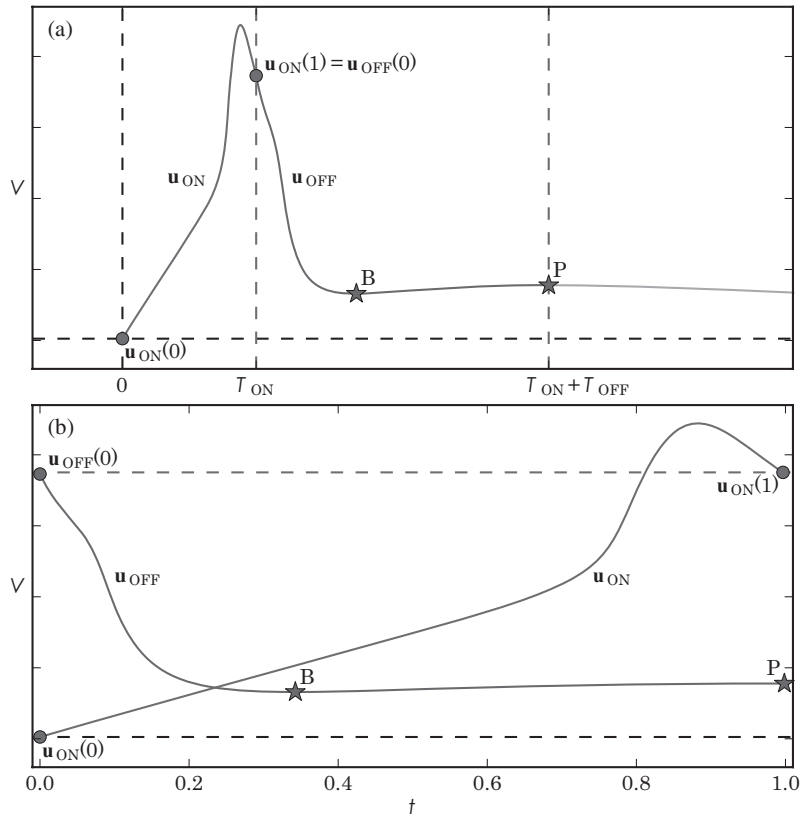


Figure 2: Illustration of how to interpret solutions to the 2PBVP (see equations 3.2–3.5); shown is a solution of equation 2.1 for which the short current injection generates a single spike and the transient response generates only an ADP. (a) The time series of $V$ for the concatenated orbit segments $\mathbf{u}_{ON}$ and $\mathbf{u}_{OFF}$ rescaled back to original time. (b) The corresponding numerical representation on the $[0, 1]$ interval. The first segment $\mathbf{u}_{ON}$ starts at the resting potential for $I_{app} = 0\,\mu\text{A/cm}^2$, as indicated by the horizontal dashed line, and is a solution of equation 3.2 with $I_{app} = 20\,\mu\text{A/cm}^2$; the total integration time is $T_{ON}$, which we set to 3 ms. The second segment $\mathbf{u}_{OFF}$ starts at the end point $\mathbf{u}_{ON}(1)$ of $\mathbf{u}_{ON}$ and is a solution of equation 3.3 with total integration time $T_{OFF}$. As explained in section 3.1, we define $T_{OFF}$ such that $\mathbf{u}_{OFF}(1)$ lies at the local maximum, denoted $P$.

over a longer time interval. Figure 2b shows the two orbit segments $\mathbf{u}_{ON}$ and $\mathbf{u}_{OFF}$ with time rescaled to the $[0, 1]$ interval.

The boundary conditions that determine $T_{OFF}$ at the onset of ADP or the onset of a new spike are explained and illustrated in the next two

sections. We do not describe here how to obtain a first solution to such 2PBVPs; this has been discussed in detail for a similar 2PBVP in Nowacki et al. (2012). Note that a different first solution must be generated each time when detecting the next onset of ADP or the next onset of a new spike.

**3.1 Identifying the Onset of ADP in a Transient Burst.** The ADP is characterized by the existence of a local minimum $B$ and a local maximum $P$, which occur after one or a series of spikes and form a small hump as shown in Figure 2a. The 2PBVP system 3.2 to 3.5 has a solution that corresponds to a response with ADP if we restrict $T_{\mathrm{OFF}}$ such that the orbit segment $\mathbf{u}_{\mathrm{OFF}}$ ends at $P$, that is, $\mathbf{u}_{\mathrm{OFF}}$ ends precisely at the point where it has a local maximum with respect to $V$. Hence, we do not fix the integration time $T_{\mathrm{OFF}}$ for $\mathbf{u}_{\mathrm{OFF}}$, but determine its value by requiring $dV/dt = 0$ at $\mathbf{u}_{\mathrm{OFF}}(1)$. This can be expressed as the boundary condition

$$f_1(\mathbf{u}_{\mathrm{OFF}}(1), \lambda, 0) = 0, \tag{3.6}$$

where $f_1$ is the first equation of system 2.1, that is, the equation for $dV/dt$.

Figure 3 shows six solutions selected from the family of orbit segments that is obtained by continuation of the 2PBVP system 3.2 to 3.6, using $g_{\mathrm{SI}}$ as the free parameter; here, we decreased $g_{\mathrm{SI}}$ from $g_{\mathrm{SI}} = 0.5\,\mathrm{mS/cm^2}$. Figure 3a shows the time series of $V$ scaled back to the original time (see also Figure 2a). The variation in $g_{\mathrm{SI}}$ has almost no effect on the orbit segment $\mathbf{u}_{\mathrm{ON}}$ of equation 3.2 that satisfies equation 3.5 with $T_{\mathrm{ON}} = 3\,\mathrm{ms}$, so that $\mathbf{u}_{\mathrm{OFF}}$ starts at almost the same point for all these orbit segments. However, the end points of $\mathbf{u}_{\mathrm{OFF}}$ change substantially, and the value for $T_{\mathrm{OFF}}$ decreases with $g_{\mathrm{SI}}$, which also corresponds to a decrease in the value of the $V$-coordinate. Figure 3b shows only the orbit segments $\mathbf{u}_{\mathrm{OFF}}$ in projection onto the $(dV/dt, V)$-plane, where we focus on the parts near the end points $\mathbf{u}_{\mathrm{OFF}}(1)$; as before, the value of the $V$-coordinate decreases with $g_{\mathrm{SI}}$. The local minima $B$ and maxima $P$ that indicate the existence of ADP are the points on $\mathbf{u}_{\mathrm{OFF}}$ with $dV/dt = 0$, which is the vertical dashed line in Figure 3b. Since we require equation 3.6, all end points $\mathbf{u}_{\mathrm{OFF}}(1) = P$ satisfy $dV/dt = 0$. Note that the local minima B also lie on the $V$-nullcline, so that each selected orbit segment also intersects the line $dV/dt = 0$ at a point $\mathbf{u}_{\mathrm{OFF}}(t) = B$ with $0 < t < 1$. The only exception is the orbit segment at the bottom in Figure 3b; this orbit segment corresponds to the solution of system 3.2 to 3.6 for which the continuation reaches a minimum value of $g_{\mathrm{SI}} \approx 0.2006\,\mathrm{mS/cm^2}$, and at this parameter value Auto detects a fold bifurcation (Kuznetsov, 1998). This is visualized in Figure 3c, where we plot only the $V$-coordinates of the local minimum $B$ and local maximum $P$ along each of the orbit segments that end at points $P$ and the lower branch to orbit segments that end at points $B$. The fold bifurcation itself corresponds to an inclination point at which $B$ and $P$ merge, which means that it marks the onset of ADP; note that the fold bifurcation seems to

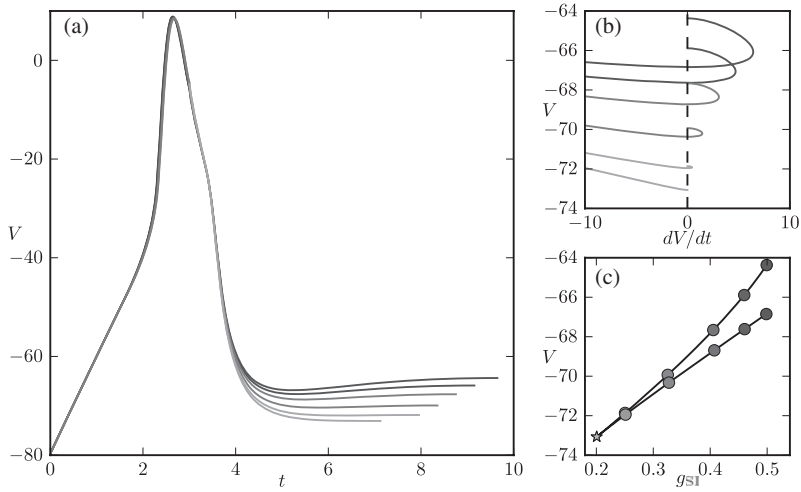


Figure 3: Continuation of the 2PBVP system, 3.2 to 3.6, as $g_{\mathrm{SI}}$ decreases. (a) Selected time series in $V$ of the $g_{\mathrm{SI}}$-dependent solutions; the orbit segment at the bottom corresponds to the smallest value of $g_{\mathrm{SI}}$ and is the response at the onset of ADP. (b) An enlargement near the $V$-nullcline (vertical dashed line) of these solutions projected onto the $(dV/dt, V)$-plane and clearly showing that all end points satisfy $dV/dt = 0$; the orbit segment at the bottom is again at the onset of ADP. (c) The value of $V$ for each point $\mathbf{u}_{\mathrm{OFF}}(t)$ that satisfies $dV/dt = 0$, illustrating that the orbit segment at the bottom in panels a and b corresponds to a fold (marked by the star), where $g_{\mathrm{SI}}$ is minimal.

lie at a cusp point, but this is an artifact of the projection, and the computed branch is actually a smooth curve.

Fold bifurcations can be detected automatically during a one-parameter continuation run with the setup in Auto. Furthermore, any detected fold bifurcation can be continued directly using a second parameter. Hence, our approach allows us to trace the onset of ADP as a curve in two parameters.

**3.2 Identifying the Onset of a Spike in a Transient Burst.** Decreasing $g_{\mathrm{SI}}$ in section 3 led to an onset of ADP at the minimum value $g_{\mathrm{SI}} \approx 0.2006\,\mathrm{mS/cm^2}$. On the other hand, we expect that increasing $g_{\mathrm{SI}}$ leads to the onset of a spike from the ADP. More precisely, we expect that the peak $P$ of ADP will rise until it reaches some critical threshold value of the membrane potential $V$; indeed, classical studies of excitability tend to associate the excitability threshold with a certain value of the membrane potential (Hodgkin & Huxley, 1952; Izhikevich, 2006; Keener & Sneyd, 2008). Hence, the naive approach would be to monitor the value of $V$ at the end point $\mathbf{u}_{\mathrm{OFF}}(1)$ in system 3.2 to 3.6 and define the onset of a burst as the point where

$g_{SI}$ is such that $\mathbf{u}_{OFF}(1)$ has reached the critical threshold of the membrane potential. There is a major disadvantage to this idea: one would have to guess what the value of the critical threshold actually is and make heuristic assumptions, for example, that the critical threshold does not depend on $g_{SI}$. Here, we explore a different approach to define the onset of a spike, which automatically establishes the critical threshold at the same time.

As we have explained (Nowacki et al., 2012), the critical threshold is characterized by a response with an elongated depolarized state of maximal duration. Nevertheless, the actual generation of a new spike takes place over an exponentially small $g_{SI}$ interval. The first such spike generation occurs for $g_{SI} \approx 0.5615\,\mathrm{mS/cm^2}$. Figure 4 illustrates the result from a continuation of the 2PBVP system 3.2 to 3.6, with $g_{SI}$ increasing from $0.5\,\mathrm{mS/cm^2}$. Here, we plot the part where the response changes dramatically, while the increase in $g_{SI} \approx 0.5615\,\mathrm{mS/cm^2}$ is only of order $O(10^{-7})$. Since Auto takes many continuation steps to capture this variation in the response, we plot the total integration time $T_{OFF}$ in Figure 4a versus the point number of the continued branch. To illustrate the deformation of the response during spike adding, we select 11 solutions along the continuation branch and plot in Figure 4b their corresponding time series in $V$ using a color gradient from dark to light as $g_{SI} \approx 0.5615\,\mathrm{mS/cm^2}$ increases. The continuation branch in Figure 4a contains three extrema where the derivative with respect to $T_{OFF}$ vanishes (marked by stars); the corresponding solutions are shown with thicker lines in Figure 4b. The orbit segment with the smallest selected $g_{SI}$ value has a local maximum with respect to $T_{OFF}$ at $T_{OFF} \approx 105.3808$ ms. Its time series is the bottom (darkest) curve in Figure 4b, shown with a thicker line to indicate that $T_{OFF}$ is at an extremum here. As $g_{SI}$ increases, the next two solutions have smaller $T_{OFF}$ values, but we observe in Figure 4b that the $V$ value at the end point $\mathbf{u}_{OFF}(1)$ rises; note that our selection includes the second extremal solution, where $T_{OFF}$ has a local minimum. The voltage at $\mathbf{u}_{OFF}(1)$ continues to rise slowly as we follow the branch in Figure 4a up to the maximum $T_{OFF} \approx 168.8113$ ms, which is again indicated by a thicker line in Figure 4b. As expected, the time series of solutions that are selected for values of $g_{SI} \approx 0.5615\,\mathrm{mS/cm^2}$ past this maximum exhibit a well-defined spike, that is, they exhibit a substantial rise in $V$ over a relatively short time interval.

Unfortunately, the numerical detection of a maximum in $T_{OFF}$ can be computationally difficult because there is no a priori bound on $T_{OFF}$. We have found a different approach that is numerically very stable and detects the onset of a spike at virtually the same $g_{SI}$ value. The substantially longer duration of the depolarized state allows the slow inward current $I_{SI}$ to inactivate almost completely. Figure 4c shows the same solution branch as in Figure 4a, but instead of $g_{SI}$, we plot the $h_{SI}$-coordinate at the end points $\mathbf{u}_{OFF}(1)$ on the horizontal axis. We observe that the inactivation $h_{SI}$ of $I_{SI}$ appears to reach a minimum exactly when $T_{OFF}$ achieves its maximum. As for $T_{OFF}$, there are three extrema for the $h_{SI}$ coordinate at $\mathbf{u}_{OFF}(1)$, which

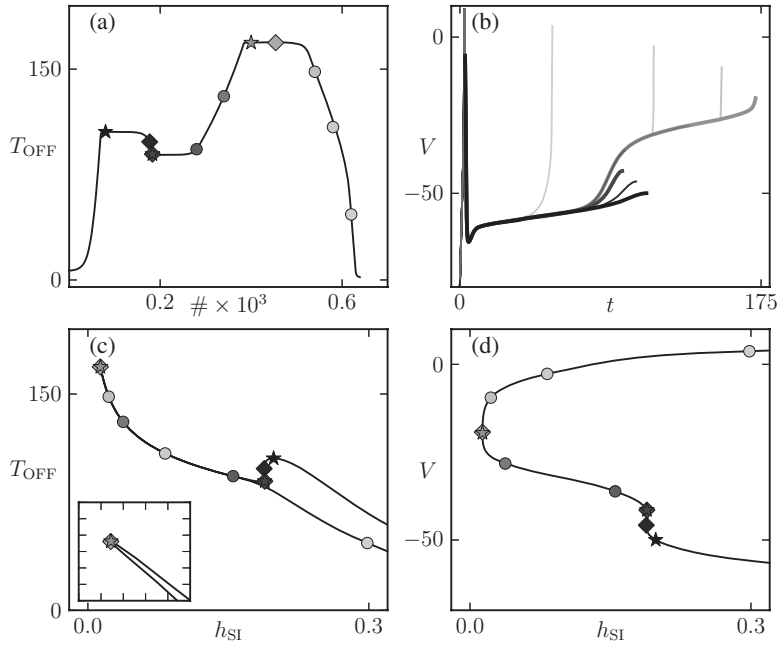


Figure 4: Continuation of the 2PBVP system 3.2 to 3.6, as $g_{\mathrm{SI}}$ increases over an exponentially small parameter interval with $g_{\mathrm{SI}} \approx 0.5615\,\mathrm{mS/cm^2}$. (a) The solution branch of the $g_{\mathrm{SI}}$-dependent family with $T_{\mathrm{OFF}}$ on the vertical axis and the point number # along the branch (in thousands) on the horizontal axis; time series for $V$ of selected orbit segments marked in panel (a) are visualized in panel (b). The extremal orbit segments with respect to the $T_{\mathrm{OFF}}$ are marked by stars in panel (a) and shown with thicker lines in panel (b). Panel (c) shows the same solution branch as in panel (a), but with the $h_{\mathrm{SI}}$-coordinate at the end points $\mathbf{u}_{\mathrm{OFF}}(1)$ on the horizontal axis. This panel illustrates that the extrema of $T_{\mathrm{OFF}}$ are located at almost the same points where $h_{\mathrm{SI}}$ at $\mathbf{u}_{\mathrm{OFF}}(1)$ is at a local minimum or maximum (marked by a diamonds). The inset in panel (c) highlights the smooth behavior near the global maximum for $T_{\mathrm{OFF}}$. Panel (d) shows the end points $\mathbf{u}_{\mathrm{OFF}}(1)$ in projection onto the $(h_{\mathrm{SI}}, V)$-plane and gives a better idea of the overall smoothness of the solution branch; again the gradient along the marked solutions serves as a guide how $g_{\mathrm{SI}}$ increases along the branch.

are marked by diamonds in Figure 4, and all three are close to the three extrema for $T_{\mathrm{OFF}}$ (marked by stars); in fact, one can distinguish only nine different solutions in Figure 4b, because two of the extrema with respect to the $h_{\mathrm{SI}}$-coordinate at $\mathbf{u}_{\mathrm{OFF}}(1)$ are virtually identical to extrema with respect to $T_{\mathrm{OFF}}$. The solution branch for the continuation of system 3.2 to 3.6 with $g_{\mathrm{SI}}$ increasing from $0.5\,\mathrm{mS/cm^2}$ to $0.6\,\mathrm{mS/cm^2}$ is perhaps best visualized

in projection of the end points $\mathbf{u}_{\mathrm{OFF}}(1)$ onto the $(h_{\mathrm{SI}}, V)$-plane as shown in Figure 4d; $g_{\mathrm{SI}}$ increases from the bottom right to the top right in this picture, and the extrema for $T_{\mathrm{OFF}}$ and $h_{\mathrm{SI}}$ are again marked by stars and diamonds, respectively. The spiking threshold, which is defined by the fact that $T_{\mathrm{OFF}}$ is globally maximal, can be viewed as the point where $h_{\mathrm{SI}}$ at $\mathbf{u}_{\mathrm{OFF}}(1)$ is minimal, which numerically occurs at the same value $g_{\mathrm{SI}} \approx 0.5615\,\mathrm{mS/cm^2}$ with a difference of $O(10^{-8})$. Numerically, it is advantageous to detect the global minimum of $h_{\mathrm{SI}}$ at the end point $\mathbf{u}_{\mathrm{OFF}}(1)$, because the $h_{\mathrm{SI}}$-coordinate at $\mathbf{u}_{\mathrm{OFF}}(1)$ is biophysically restricted to the interval $[0, 1]$ and cannot grow unboundedly. As shown in Figure 4, not only the $g_{\mathrm{SI}}$ value but also the corresponding value for $V$ at $\mathbf{u}_{\mathrm{OFF}}(1)$ and the total integration time $T_{\mathrm{OFF}}$ are very similar at this minimum of $h_{\mathrm{SI}}$.

The behavior of the $h_{\mathrm{SI}}$ coordinate at $\mathbf{u}_{\mathrm{OFF}}(1)$ is representative of the behavior of the two slow variables $h_{\mathrm{SI}}$ and $m_{\mathrm{SO}}$ in our system, and extrema of either the $h_{\mathrm{SI}}$ or the $m_{\mathrm{SO}}$ coordinates at $\mathbf{u}_{\mathrm{OFF}}(1)$ can be used to detect the onset of a spike. We chose to work with the $h_{\mathrm{SI}}$ coordinate because the change of $h_{\mathrm{SI}}$ in the low-voltage region is more profound than that of $m_{\mathrm{SO}}$, which is also slightly slower (see Table 1).

For the setup in Auto, we solve system 3.2 to 3.6 and detect the minimum in $h_{\mathrm{SI}}$ at $\mathbf{u}_{\mathrm{OFF}}(1)$ using an optimization approach. To this end, we introduce a parameter denoted $h^e_{\mathrm{OFF}}$ and add the boundary condition

$$[0, 0, 0, 0, 1] * \mathbf{u}_{\mathrm{OFF}}(1) - h^e_{\mathrm{OFF}} = 0 \tag{3.7}$$

to system 3.2 to 3.6. Here, the vector product $[0, 0, 0, 0, 1] * \mathbf{u}_{\mathrm{OFF}}(1)$ extracts the $h_{\mathrm{SI}}$-coordinate from $\mathbf{u}_{\mathrm{OFF}}(1)$. We now allow $h^e_{\mathrm{OFF}}$ to vary freely during the continuation; note that $T_{\mathrm{OFF}}$ also remains a free parameter in this 2PBVP system. The advantage of such a setup is that Auto can detect folds with respect to the parameter $h^e_{\mathrm{OFF}}$; since the boundary condition 3.7 is satisfied only when $h^e_{\mathrm{OFF}}$ equals the value of the $h_{\mathrm{SI}}$ coordinate at the end point of a solution $\{(\mathbf{u}_{\mathrm{ON}}(t), \mathbf{u}_{\mathrm{OFF}}(t)) \mid 0 \le t \le 1\}$ for system 3.2 to 3.6, this means that Auto effectively detects the extrema of $h_{\mathrm{SI}}$ at the end point $\mathbf{u}_{\mathrm{OFF}}(1)$.

Figure 5 illustrates that our method for detecting the onset of a spike also works for solutions with more than one spike in their transient response. The next two spike generations occur over exponentially small parameter intervals at $g_{\mathrm{SI}} \approx 0.5697\,\mathrm{mS/cm^2}$ and $g_{\mathrm{SI}} \approx 0.6183\,\mathrm{mS/cm^2}$; the associated continuation runs are shown in rows 1 and 2 of Figure 5, respectively. The starting solutions for these runs were found as follows. We selected two nearby solutions from the branch computed for Figure 4, namely, at $g_{\mathrm{SI}} = 0.5690\ \mathrm{mS/cm^2}$ and at $g_{\mathrm{SI}} = 0.6180\ \mathrm{mS/cm^2}$. These parameter values are well past the exponentially small $g_{\mathrm{SI}}$-interval during which the second spike is generated, so that both solutions are orbit segments with one spike followed by the rising part of the next spike up to the (local) maximum. We extended these orbit segments for $g_{\mathrm{SI}} = 0.5690\ \mathrm{mS/cm^2}$ and

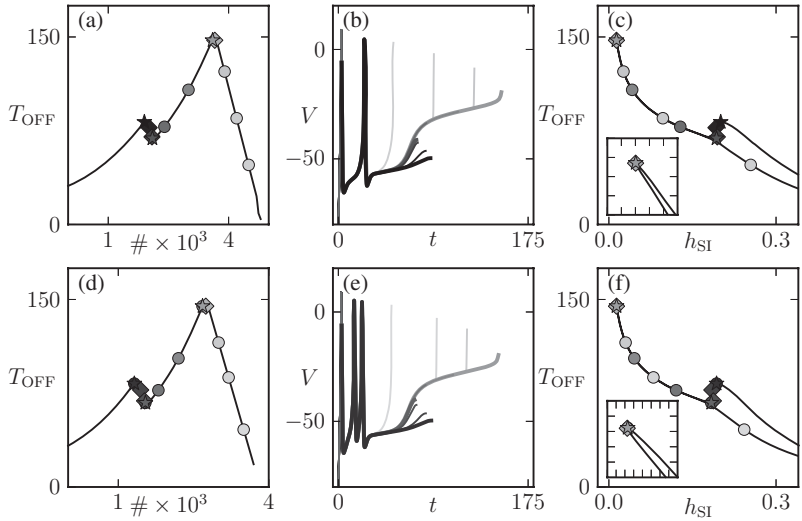


Figure 5: Continuation of families with two and three spikes that solve system 3.2 to 3.6 as a function of $g_{\mathrm{SI}}$. (a–c) The branch of two-spike solutions continued past the critical threshold at $g_{\mathrm{SI}} \approx 0.5697\,\mathrm{mS/cm^2}$. (d–f) The branch of three-spike solutions, for which the critical threshold lies at $g_{\mathrm{SI}} \approx 0.6183\,\mathrm{mS/cm^2}$. Panels (a) and (d) show the solution branches of the $g_{\mathrm{SI}}$-dependent families with $T_{\mathrm{OFF}}$ on the vertical axis and the point number # along the branch (in thousands) on the horizontal axis; time series for $V$ of selected orbit segments as marked in these panels are visualized in panels (b) and (e), respectively, colored from dark to light as $g_{\mathrm{SI}}$ increases (exponentially small). The extremal orbit segments with respect to the $T_{\mathrm{OFF}}$ are marked by stars on the solution branches and shown with thicker lines in panels (b) and (e). Panels (c) and (f) show $T_{\mathrm{OFF}}$ versus the $h_{\mathrm{SI}}$-coordinate at the end points $\mathbf{u}_{\mathrm{OFF}}(1)$ on the horizontal axis and illustrate that these other two solution types also have the extrema of $T_{\mathrm{OFF}}$ located at almost the same points where $h_{\mathrm{SI}}$ at $\mathbf{u}_{\mathrm{OFF}}(1)$ is at a local minimum or maximum (marked by a diamonds). The insets highlight the smooth behavior near the global maximum for $T_{\mathrm{OFF}}$. Compare also with 4.

$g_{\mathrm{SI}} = 0.6180\ \mathrm{mS/cm^2}$ by increasing $T_{\mathrm{OFF}}$ such that they are solutions of system 3.2 to 3.6 that exhibit two and three spikes, respectively, before ending in a local maximum of the ADP at $\mathbf{u}_{\mathrm{OFF}}(1)$. Figures 5a and 5d correspond to Figure 4a and show the total integration time $T_{\mathrm{OFF}}$ versus the point number of the continued branch. The time series in $V$ of selected solutions as marked in Figures 5a and 5d are shown in Figures 5b and 5e, respectively; the thicker curves indicate a solution for which $T_{\mathrm{OFF}}$ achieves a local maximum or minimum, which are marked by stars on the continuation branch. Figures 5c and 5f show the continuation branch by plotting $T_{\mathrm{OFF}}$ versus the $h_{\mathrm{SI}}$-coordinate

at the end point $\mathbf{u}_{\mathrm{OFF}}(1)$, as was done in Figure 4c for the one-spike solution branch. This last projection illustrates that extrema of $h_{\mathrm{SI}}$ at $\mathbf{u}_{\mathrm{OFF}}(1)$ (marked by diamonds) appear to be closely related to extrema of $T_{\mathrm{OFF}}$ (marked by stars), and the global minimum of $h_{\mathrm{SI}}$ at $\mathbf{u}_{\mathrm{OFF}}(1)$ is a good approximation for the global maximum of $T_{\mathrm{OFF}}$ that characterizes the onset of the next spike.

## 4 Computing Boundaries between Transient Bursting Patterns

Our numerical methods for detecting the $g_{\mathrm{SI}}$ values at which the system exhibits the onset of ADP or the onset of a spike are all based on detecting fold bifurcations for a 2PBVP in Auto (Doedel, 1981; Doedel & Oldeman, 2009). This means that we can subsequently use fold continuation in Auto to trace the onsets of APD or a spike as curves in a two-parameter plane. Such curves would form the boundaries between different bursting behaviors of the model. We illustrate this by computing the boundary curves in the $(g_{\mathrm{FO}}, g_{\mathrm{SI}})$-plane, because the magnitude of $g_{\mathrm{FO}}$ influences the amplitude of ADP and, thus, the overall excitability (Nowacki et al., 2011).

There are two types of curves: the onset of ADP and the onset of a spike. In order to compute a curve in the $(g_{\mathrm{FO}}, g_{\mathrm{SI}})$-plane that forms a separatrix between regions with and without ADP, we start from a solution of the 2PBVP system 3.2 to 3.6 that has a fold with respect to $g_{\mathrm{SI}}$; here, only $g_{\mathrm{SI}}$ and $T_{\mathrm{OFF}}$ are free parameters. A curve that corresponds to the onset of a new spike, on the other hand, can be started from a solution of the 2PBVP system 3.2 to 3.7, where $h^e_{\mathrm{OFF}}$, $g_{\mathrm{SI}}$, and $T_{\mathrm{OFF}}$ are the free parameters. We then include $g_{\mathrm{FO}}$ in the list of free parameters and solve the 2PBVP system in Auto with the additional constraint that the system remains at a fold point with respect to $g_{\mathrm{SI}}$ (for onset of ADP) or $h^e_{\mathrm{OFF}}$ (for onset of a new spike); the corresponding extended 2PBVP system is generated automatically in Auto.

Figure 6 shows the results of the fold continuation in the $(g_{\mathrm{FO}}, g_{\mathrm{SI}})$-plane. The bifurcation diagram is shown in Figure 6a, and examples of responses for parameter values in the different regions are shown in Figures 6b to 6m. The solid curves in Figure 6a are the fold continuation branches. We are interested only in the positive quadrant, $g_{\mathrm{FO}}, g_{\mathrm{SI}} \geq 0\,\mathrm{mS/cm^2}$. Furthermore, the bursting regime is bounded from above by the (dashed green) curve of Hopf bifurcations of the full system, 2.1. On the other side of this Hopf curve, any short-current injection drives the system into a continuous (tonic) spiking state due to the presence of a periodic attractor. For reasons that we explain later, we stop the continuation when $g_{\mathrm{FO}}$ reaches the value $g_{\mathrm{FO}} = 17\,\mathrm{mS/cm^2}$ (dashed vertical line on the right). The bottom solid curve corresponds to the onset of ADP; representative responses on either side of this curve in Figures 6b and 6c illustrate the transition from a response with no ADP to one with the distinctive hump at the end of the spike. The other solid curves correspond to onsets of a new spike and the dark-to-light coloring indicates the increase in the number of spikes. We

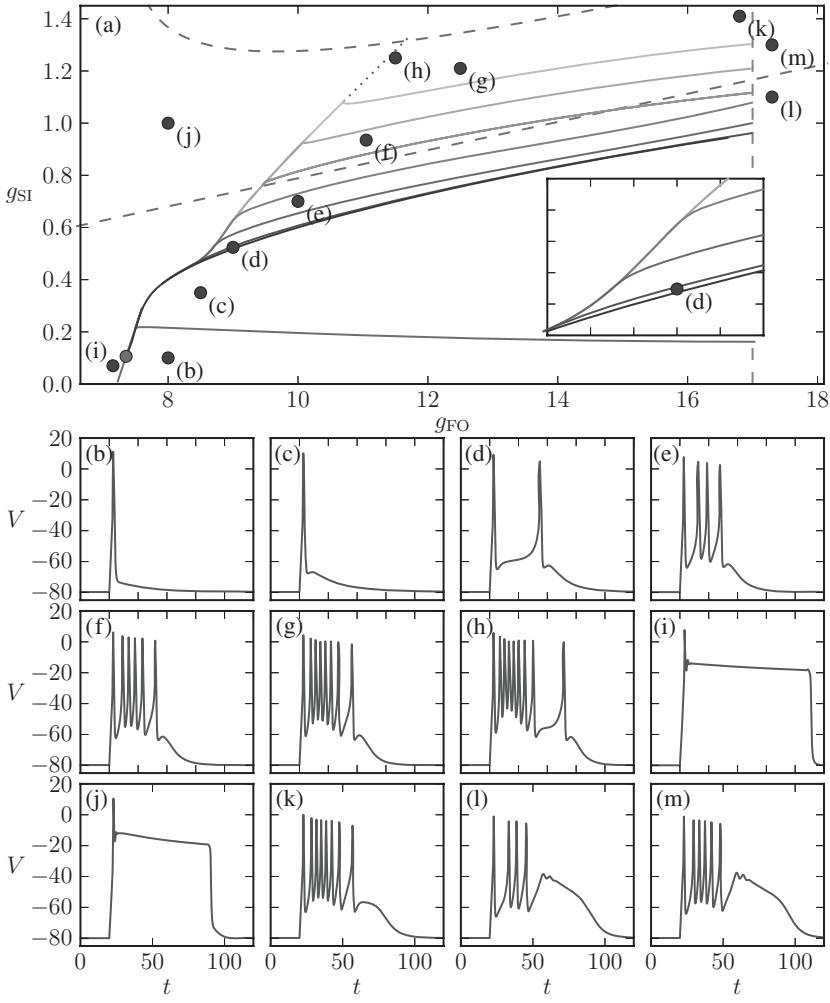


Figure 6: Regions of different model behavior in the $(g_{FO}, g_{SI})$-plane established by fold continuation of system 3.2 to 3.6 or with the additional boundary condition 3.7. (a) The bifurcation diagram, with an enlargement of the two-spike burst region in the inset, and panels (b)–(m) responses of system 2.1 for the parameter values as marked by dots in panel (a). The solid curves are the onsets of a spike, and the color gets lighter as the number of spikes increases. The solid curve at the bottom corresponds to the onset of ADP and the dashed curve at the top to Hopf and the dashed curve in the middle to saddle-node bifurcation of the full system 2.1. We stopped the computations at the dashed vertical line on the right; the open circle marks the left end point of the continuation of onsets of a spike.

continued folds of bursts with one to seven spikes; representative responses from the regions where the transient burst has an even number of spikes are shown in Figures 6d to 6g. We show only the first curve of onset of ADP, because the continuation of onset of ADP for solutions that already exhibit more than one spike leads to curves that lie virtually on top of the branches corresponding to onsets of a new spike. We computed some of these additional ADP boundaries, but the other regions of responses with no ADP are so small that we decided to ignore the distinction between such regimes altogether. Note that the curves of onsets of the second and third spikes lie very close together. Both curves are computed by fold continuation in Auto, but the solutions along these two branches are very different when considered in the full solution space $(\mathbf{u}_{\mathrm{ON}}(t), \mathbf{u}_{\mathrm{OFF}}(t), h^e_{\mathrm{OFF}}, g_{\mathrm{SI}}, T_{\mathrm{OFF}}, g_{\mathrm{FO}})$. Hence, our method successfully distinguishes the two curves and establishes each boundary accurately; such boundary curves are much more difficult to determine using brute-force simulations.

The advantage of our approach is that it also successfully continues the different curves when they accumulate on each other, as is the case in the direction with $g_{\mathrm{FO}}$ decreasing. In fact, all seven computed curves merge on the left and also merge with the boundary of ADP (the solid horizontal line at the bottom). Again, the fold continuation in Auto views each curve as a distinct family in the full solution space $(\mathbf{u}_{\mathrm{ON}}(t), \mathbf{u}_{\mathrm{OFF}}(t), h^e_{\mathrm{OFF}}, g_{\mathrm{SI}}, T_{\mathrm{OFF}}, g_{\mathrm{FO}})$ that is well separated from the other burst families, so that the accumulation of curves is numerically not an issue.

The continuation for each of the branches that characterize the onset of a spike stops on the boundary of ADP, approximately at the point marked by an open circle in Figure 6a. Only the boundary of ADP extends to the $g_{\mathrm{FO}}$-axis. This open circle in Figure 6a marks the point where the $h_{\mathrm{SI}}$-coordinate at $\mathbf{u}_{\mathrm{OFF}}(1)$ reaches zero. Indeed, the curves of onsets of a spike are computed by continuation of a minimum $h^e_{\mathrm{OFF}}$ in the $h_{\mathrm{SI}}$-coordinate at $\mathbf{u}_{\mathrm{OFF}}(1)$, and this minimum $h^e_{\mathrm{OFF}}$ decreases as $g_{\mathrm{FO}}$ and/or $g_{\mathrm{SI}}$ decrease. Since $h_{\mathrm{SI}}$ is constrained by equation 2.2 to the biological range $[0, 1]$, it is not possible to continue the minimum $h^e_{\mathrm{OFF}}$ past zero. In contrast, the onset of ADP takes place for much higher values of $h_{\mathrm{SI}}$ at $\mathbf{u}_{\mathrm{OFF}}(1)$ so that the continuation of this boundary proceeds until $g_{\mathrm{SI}} = 0$.

We computed seven curves of onsets of a spike, with the last curve marking the transition between seven and eight spikes in a burst. As shown in Figure 6a, these boundary curves accumulate in such a way that a left boundary is formed by consecutive segments of the boundary curves. We extrapolated this boundary (the dotted line) up to the dashed Hopf curve (at the top of the figure) indicating the expected extent of the region with spike-adding behaviour. For example, the response in Figure 6h is for a $(g_{\mathrm{FO}}, g_{\mathrm{SI}})$ pair that lies very close but to the right of this extrapolated boundary. This response is a transient burst with nine spikes; hence, there exists at least one additional curve of onset of a new spike before reaching the Hopf curve.

To the left of the (extrapolated) boundary of the spiking regime, the response is no longer a burst, but exhibits a depolarized plateau with an indistinguishable number of spikes that have extremely small amplitudes; two representative responses chosen far apart from each other are shown in Figures 6i and 6j. This regime is characterized by a slow passage through a Hopf bifurcation of the fast subsystem (for more details, see Baer, Erneux, & Rinzel, 1989; Izhikevich, 2006; Ermentrout & Terman, 2010; Desroches, Guckenheimer, Krauskopf, Kuehn, Osinga, & Wechselberger, 2012). Note that this behavior is still transient and the solution eventually returns to the resting membrane potential.

The dashed curve through the middle in Figure 6a is a curve of saddle-node bifurcations of the full system 2.1; above this curve, an additional pair of equilibria coexists with the resting potential, but only the resting potential is a stable equilibrium. This curve does not act as a boundary for a particular type of bursting, but the presence of the two equilibria alters the nature of the spike-adding mechanism and $T_{\mathrm{OFF}}$ actually goes to infinity at the critical threshold, which is now characterized by a (transiently induced) heteroclinic connection to one of the saddle equilibria (see Nowacki et al., 2012, for more details). While the spike-adding mechanism changes, the responses of the system on either side of the middle dashed curve of saddle node bifurcations inside each of the bursting regions are qualitatively the same. Our approach for finding the onsets of a spike, where we detect a minimum for the $h_{\mathrm{SI}}$ coordinate at $\mathbf{u}_{\mathrm{OFF}}(1)$ instead of a maximum for $T_{\mathrm{OFF}}$, also works for $(g_{\mathrm{FO}}, g_{\mathrm{SI}})$ values above this curve of saddle node bifurcations, though the solution is a coarser approximation and only the $(g_{\mathrm{FO}}, g_{\mathrm{SI}})$ values of the actual critical threshold are found accurately here.

We decided to stop the computations as soon as we reached $g_{\mathrm{FO}} = 17\,\mathrm{mS/cm^2}$. For $g_{\mathrm{FO}} > 17\,\mathrm{mS/cm^2}$ the burst response develops a plateau-like ADP that contains a number of small-amplitude oscillations. The response shown in Figure 6k, for $g_{\mathrm{FO}}$ just below $17\,\mathrm{mS/cm^2}$ illustrates the formation of the plateau-like ADP, and Figures 6l and 6m are examples of what the response looks like for $g_{\mathrm{FO}} > 17\,\mathrm{mS/cm^2}$. The nature of the transient response changes in a way that is different from adding a new spike, and it is more difficult to define the number of spikes in the burst. Other behaviors may arise for $g_{\mathrm{SI}} > 17\,\mathrm{mS/cm^2}$ that have not been analyzed here. Note that the occurrence of small-amplitude oscillations on top of the ADP can lead to convergence problems in Auto, and it is challenging to continue the branches for larger values of $g_{\mathrm{FO}}$. These numerical difficulties are due to the fact that there now exist several nearby solutions that all satisfy boundary condition 3.6, which requires that the end point $\mathbf{u}_{\mathrm{OFF}}(1)$ lies at an extremum in $V$. Indeed, for slightly larger $T_{\mathrm{OFF}}$, there exist solutions of the 2PBVP 3.2 to 3.7 that end at a minimum or maximum in $V$ of either one of these small-amplitude oscillations; these solutions all lie close to each other, even when considering the full solution space $(\mathbf{u}_{\mathrm{ON}}(t), \mathbf{u}_{\mathrm{OFF}}(t), h^e_{\mathrm{OFF}}, g_{\mathrm{SI}}, T_{\mathrm{OFF}}, g_{\mathrm{FO}})$. Figure 6a gives a good overview of

the sensitivity of the bursting behavior in our model to changes in the parameters $g_{SI}$ and $g_{FO}$. We find that changes in $g_{SI}$ have a much larger effect on the bursting behavior than changes in $g_{FO}$. This means that the low-voltage-activated slow inward currents have a larger impact on excitability in our model. We distinguish three large regimes in our region of interest: one-spike responses with ADP, one-spike responses without ADP, and the combined regions of responses with multiple spikes. As shown in Figure 6a, the responses with just one spike and with ADP appear to cover the largest area in the parameter plane. Our simplified model has been derived based on a more detailed, biophysical model (Nowacki et al., 2011) calibrated using data from Brown and Randall (2009) and agrees with experimental recordings indicating that the response with just one spike followed by an ADP is the most robust (Brown & Randall, 2009). In addition, the region with no ADP after the first spike is relatively large, which is in line with the experimental results reported by Brown and Randall (2009), Golomb et al. (2006), and Yaari, Yue, and Su (2007).

## 5 Discussion

In this letter, we presented a continuation-based numerical method for the detection of the onsets of after-depolarization (ADP) as well as a spike in a transient burst. We defined a two-point boundary value problem (2PBVP) that identifies such onsets as special orbit segments that are determined as fold bifurcations in continuation packages such as Auto (Doedel, 1981; Doedel & Oldeman, 2009). The 2PBVP formulation mirrors the stimulation protocols used in electrophysiological experimental studies, so that the analysis of our model can be related directly to the experimental results. We have used a relatively simple model and protocol to illustrate our approach, but our 2PBVP formulation can be adapted, in principle, to suit onsets of other phenomena in applications involving transient responses generated by different stimulation protocols. The advantage of using a model is that we can analyze the sensitivity of the model to any choice of parameters. In particular, we can make predictions for parameters that are hard, if not impossible, to control using experimental techniques, such as time constants or membrane capacitance.

For the detection of onset of ADP, we use the formal definition of ADP as a local maximum of the membrane potential $V$ and defined the 2PBVP as a system for which the solutions are orbit segments that follow the stimulation protocol and end at the local maximum identifying the ADP. The disappearance of this local maximum, as a parameter is varied, occurs through an inflection point, where the local maximum merges with the preceding local minimum. During the continuation of the 2PBVP, the inflection point is detected as a fold with respect to the parameter. The onset of a spike is more challenging because there is no parameter-independent definition of a spiking threshold. Rather than setting an arbitrary critical threshold for

$V$, we use our findings in Nowacki et al. (2012) that spike adding occurs via a canard-like mechanism in models of Hodgkin-Huxley type that exhibit different timescales (see also Terman, 1991, 1992, and Guckenheimer & Kuehn, 2009). This means that the onset of a new spike coincides with a maximum in the time $T_{\mathrm{OFF}}$ that it takes the transient response to reach the local maximum of ADP as it relaxes back to the resting potential. In this letter, we argue that the drastic increase in $T_{\mathrm{OFF}}$, which indicates the onset of a new spike, must be accompanied by a decrease in the inactivation $h_{\mathrm{SI}}$ of the slow inward current. From a numerical point of view, it is better to detect a minimum in this bounded variable $h_{\mathrm{SI}}$ at the end point of the orbit segment that solves our 2PBVP, and we formulate it such that we can again detect this minimum as a fold point on the branch; note that this fold is not with respect to the continuation parameters.

We have shown that the detected onsets of ADP and a spike can be continued in a two-parameter plane to establish regions of different transient behavior. Identification of such regions corresponds to a parameter sensitivity analysis of transient bursting patterns found in this class of models. Our analysis shows that there exists a large area in the parameter plane for which the response exhibits a highly depolarized state (see the responses in Figures 6i and 6j). Similar behavior has been observed experimentally (Golomb et al., 2006) by applying the $K^+$-channel blocker linopirdine. Such a prolonged depolarized state is potentially very dangerous for the cell because the membrane potential is away from the resting state. This may lead to excessive influx of $Ca^{2+}$ that can reach toxic levels. We find that this region is relatively large and directly adjacent to the physiological bursts regime. Our findings indicate that hyperexcitable cells (that fire many spikes) could easily be driven into such a potentially dangerous state. We note that an increase in $g_{\mathrm{FO}}$ could also be dangerous, as it decreases excitability and leads to a prominent ADP with small oscillations (see the responses in Figures 6l and 6m). Such a prolonged ADP can have a similar effect on the influx of $Ca^{2+}$. Hence, this behavior could possibly be detrimental for the cell as well.

## Acknowledgments

The research for this letter was done while J.N. was a Ph.D. student at the University of Bristol, supported by grant EP/E032249/1 from the Engineering and Physical Sciences Research Council (EPSRC). The research of K.T-A. was supported by EPSRC grant EP/I018638/1 and that of H.M.O. by grant UOA0718 of the Royal Society of NZ Marsden Fund.

## References

Andersen, P., Morris, R., Amaral, D., Bliss, T., & O'Keefe, J. (2007). *The hippocampus book*. New York: Oxford University Press.

Baer, S. M., Erneux, T., & Rinzel, J. (1989). The slow passage through a Hopf bifurcation: Delay, memory effects, and resonance. *SIAM J. Appl. Math.*, *49*(1), 55–71.

Brown, J. T., Chin, J., Leiser, S. C., Pangalos, M. N., & Randall, A. D. (2011). Altered intrinsic neuronal excitability and reduced Na(+) currents in a mouse model of Alzheimer's disease. *Neurobiology of Aging*, *32*(11), 2109.e1–2109.e14.

Brown, J. T., & Randall, A. D. (2009). Activity-dependent depression of the spike afterdepolarization generates long-lasting intrinsic plasticity in hippocampal CA3 pyramidal neurons. *J. Physiology*, *587*(6), 1265–1281.

Dankowicz, H., & Schilder, F. (2009). *COCO: General-purpose tools for continuation and bifurcation analysis of dynamical systems*. http://sourceforge.net/projects/cocotools

Dankowicz, H., & Schilder, F. (2011). An extended continuation problem for bifurcation analysis in the presence of constraints. *ASME J. Comp. Nonl. Dyn.*, *6*(3), 031003.

Desroches, M., Guckenheimer, J., Krauskopf, B., Kuehn, C., Osinga, H. M., & Wechselberger, M. (2012). Mixed-mode oscillations with multiple time scales. *SIAM Review*, *54*(2), 211–288.

Doedel, E. J. (1981). AUTO: A program for the automatic bifurcation analysis of autonomous systems. *Congressus Numerantium*, *30*, 265–284.

Doedel, E. J., & Oldeman, B. E. (2009). *AUTO-07p Version 0.7: Continuation and bifurcation software for ordinary differential equations*. Montreal: Department of Computer Science, Concordia University. http://cmvl.cs.concordia.ca/auto/

Epsztein, J., Brecht, M., & Lee, A. K. (2011). Intracellular determinants of hippocampal CA1 place and silent cell activity in a novel environment. *Neuron*, *70*(1), 109–120.

Ermentrout, G. B., & Terman, D. H. (2010). *Mathematical foundations of neuroscience*. New York: Springer-Verlag.

Golomb, D., Yue, C., & Yaari, Y. (2006). Contribution of persistent $Na^+$ current and M-type $K^+$ current to somatic bursting in CA1 pyramidal cells: Combined experimental and modeling study. *J. Neurophysiology*, *96*(4), 1912–1926.

Govaerts, W., & Dhooge, A. (2002). Bifurcation, bursting and spike generation in a neural model. *Int. J. Bifurcation and Chaos*, *12*(8), 1731–1741.

Guckenheimer, J., Gueron, S., & Harris-Warrick, R. M. (1993). Mapping the dynamics of a bursting neuron. *Philos. Trans. R. Soc. Lond., B, Biol. Sci.*, *341*(1298), 345–359.

Guckenheimer, J., & Kuehn, C. (2009). Computing slow manifolds of saddle type. *SIAM J. Appl. Dyn. Sys.*, *8*(3), 854–879.

Guckenheimer, J., Tien, J. H., & Willms, A. R. (2005). Bifurcations in the fast dynamics of neurons: Implications for bursting. In S. Coombes & P. C. Bressloff (Eds.), *Bursting: The genesis of rhythm in the nervous system* (pp. 89–122). Singapore: World Scientific Publishing.

Harvey, C. D., Collman, F., Dombeck, D. A., & Tank, D. W. (2009). Intracellular dynamics of hippocampal place cells during virtual navigation. *Nature*, *461*(7266), 941–946.

Hodgkin, A. L., & Huxley, A. F. (1952). A quantitive description of membrane current and its application to conduction and excitation in nerve. *J. Physiology*, *105*(117), 500–544.

Hunter, J. (2007). Matplotlib: A 2D graphics environment. *Computing in Science and Engineering*, *9*(3), 90–95.

Izhikevich, E. M. (2000). Neural excitability, spiking and bursting. *Int. J. Bifurcation and Chaos*, *10*(6), 1171–1266.

Izhikevich, E. M. (2006). *Dynamical systems in neuroscience: The geometry of excitability and bursting*. Cambridge, MA: MIT Press.

Keener, J. P., & Sneyd, J. (2008). *Mathematical physiology: Cellular physiology*. New York: Springer-Verlag.

Krahe, R., Gabbiani, F. (2004). Burst firing in sensory systems. *Nature Reviews Neuroscience*, *5*(1), 13–23.

Kuznetsov, Yu. A. (1998). *Elements of applied bifurcation theory*. New York: Springer-Verlag.

Lee, A. K., Manns, I. D., Sakmann, B., & Brecht, M. (2006). Whole-cell recordings in freely moving rats. *Neuron*, *51*(4), 399–407.

Llinás, R. R. (1988). The intrinsic electrophysiological properties of mammalian neurons: Insights into central nervous system function. *Science*, *242*(4886), 1654–1664.

Martinez-Conde, S., Macknik, S. L., & Hubel, D. H. (2002). The function of bursts of spikes during visual fixation in the awake primate lateral geniculate nucleus and primary visual cortex. *Proc. Natl. Acad. of Sciences*, *99*(21), 13920–13925.

McCormick, D. A., & Contreras, D. (2001). On the cellular and network bases of epileptic seizures. *Annual Review of Physiology*, *63*(1), 815–846.

Nowacki, J., Osinga, H. M., Brown, J. T., Randall, A. D., & Tsaneva-Atanasova, K. T. (2011). A unified model of CA1/3 pyramidal cells: An investigation into excitability. *Progr. Biophysics and Molecular Biology*, *105*(1–2), 34–48.

Nowacki, J., Osinga, H. M., & Tsaneva-Atanasova, K. T. (2012). Dynamical systems analysis of spike-adding mechanisms in transient bursts. *J. Mathematical Neuroscience*, *2*, 7.

Oliphant, T. (2007). Python for scientific computing. *Computing in Science and Engineering*, *9*(3), 10–20.

Osinga, H. M., & Tsaneva-Atanasova, K. T. (2010). Dynamics of plateau bursting depending on the location of its equilibrium. *J. Neuroendocrinology*, *22*(12), 1301–1314.

Rinzel, J. (1985). Bursting oscillations in an excitable membrane model. In B. D. Sleeman & R. J. Jarvis (Eds.), *Ordinary and partial differential equations* (pp. 304–316). Berlin: Springer-Verlag.

Rinzel, J. (1987). A formal classification of bursting mechanisms in excitable systems. In *Int. Congress of Mathematicians* (pp. 1578–1593).

Terman, D. H. (1991). Chaotic spikes arising from a model of bursting in excitable membranes. *SIAM J. Appl. Math.*, *51*(5), 1418–1450.

Terman, D. H. (1992). The transition from bursting to continuous spiking in excitable membrane models. *J. Nonlinear Science*, *2*(2), 135–182.

Thomas, M. J., Watabe, A. M., Moody, T. D., Makhinson, M., & O'Dell, T. J. (1998). Postsynaptic complex spike bursting enables the induction of LTP by theta frequency synaptic stimulation. *J. Neuroscience*, *18*(18), 7118–7126.

Tsaneva-Atanasova, K. T., Osinga, H. M., Riess, T., & Sherman, A. (2010). Full system bifurcation analysis of endocrine bursting models. *J. Theoretical Biology*, *264*, 1133–1146.

Tsaneva-Atanasova, K. T., Sherman, A., van Goor, F., & Stojilkovic, S. S. (2007). Mechanism of spontaneous and receptor-controlled electrical activity in pituitary somatotrophs: Experiments and theory. *J. Neurophysiology*, *98*(1), 131–144.

van Elburg, R. A. J., & van Ooyen, A. (2010). Impact of dendritic size and dendritic topology on burst firing in pyramidal cells. *PLoS Computational Biology*, *6*(5), e1000781.

Yaari, Y., Yue, C., & Su, H. (2007). Recruitment of apical dendritic T-type $Ca^{2+}$ channels by backpropagating spikes underlies de novo intrinsic bursting in hippocampal epileptogenesis. *J. Physiology*, *580*(2), 435–450.

Yue, C., Remy, S., Su, H., Beck, H., & Yaari, Y. (2005). Proximal persistent $Na^{+}$ channels drive spike afterdepolarizations and associated bursting in adult CA1 pyramidal cells. *J. Neuroscience*, *25*(42), 9704–9720.

Yue, C., & Yaari, Y. (2004). KCNQ/M channels control spike afterdepolarization and burst generation in hippocampal neurons. *J. Neuroscience*, *24*(19), 4614–4624.

---

Received July 20, 2012; accepted October 31, 2012.